Early intraneuronal amyloid triggers neuron-derived inflammatory signaling in APP transgenic rats and human brain

Lindsay A. Welikovitch[a], Sonia Do Carmo[b], Zsófia Maglóczky[c], Janice C. Malcolm[d], János Lőke[e], William L. Klein[f], Tamás Freund[g], and A. Claudio Cuello[a,b,d,h,1]

[a]Department of Neurology and Neurosurgery, McGill University, Montreal, QC H3G 1Y6, Canada; [b]Department of Pharmacology and Therapeutics, McGill University, Montreal, QC H3G 1Y6, Canada; [c]Human Brain Research Laboratory, Institute of Experimental Medicine of the Hungarian Academy of Sciences, 1051 Budapest, Hungary; [d]Department of Anatomy and Cell Biology, McGill University, Montreal, QC H3G 1Y6, Canada; [e]Department of Psychiatry, Szent Borbála Hospital, 2800 Tatabánya, Hungary; [f]Department of Neurobiology, Northwestern University, Evanston, IL 60208; [g]Laboratory of Cerebral Cortex Research, Institute of Experimental Medicine of the Hungarian Academy of Sciences, 1051 Budapest, Hungary; and [h]Department of Pharmacology, University of Oxford, OX1 2JD Oxford, Oxford, United Kingdom

Edited by Tomas G. M. Hökfelt, Karolinska Institutet, Stockholm, Sweden, and approved February 7, 2020 (received for review August 22, 2019)

Chronic inflammation during Alzheimer's disease (AD) is most often attributed to sustained microglial activation in response to amyloid-β (Aβ) plaque deposits and cell death. However, cytokine release and microgliosis are consistently observed in AD transgenic animal models devoid of such pathologies, bringing into question the underlying processes that may be at play during the earliest AD-related immune response. We propose that this plaque-independent inflammatory reaction originates from neurons burdened with increasing levels of soluble and oligomeric Aβ, which are known to be the most toxic amyloid species within the brain. Laser microdissected neurons extracted from preplaque amyloid precursor protein (APP) transgenic rats were found to produce a variety of potent immune factors, both at the transcript and protein levels. Neuron-derived cytokines correlated with the extent of microglial activation and mobilization, even in the absence of extracellular plaques and cell death. Importantly, we identified an inflammatory profile unique to Aβ-burdened neurons, since neighboring glial cells did not express similar molecules. Moreover, we demonstrate within disease-vulnerable regions of the human brain that a neuron-specific inflammatory response may precede insoluble Aβ plaque and tau tangle formation. Thus, we reveal the Aβ-burdened neuron as a primary proinflammatory agent, implicating the intraneuronal accumulation of Aβ as a significant immunological component in the AD pathogenesis.

intraneuronal Aβ | neuronal inflammation | preplaque pathology | Alzheimer's disease

Neuroinflammation in Alzheimer's disease (AD) has classically been regarded as a glial- and plaque-driven phenomenon: Activated microglia become coordinately recruited toward extracellular amyloid-β (Aβ) plaques, releasing toxic proinflammatory molecules and inciting neuronal damage (1–4). This overt inflammatory reaction was initially characterized as a secondary effect of advanced plaque deposition and ongoing neurodegeneration. However, reports from numerous epidemiological studies have since demonstrated that long-term use of nonsteroidal antiinflammatory drugs (NSAIDs) in patients with rheumatoid arthritis lowers the risk of developing AD (5), suggesting that inflammation may in fact be an earlier component of the AD continuum than previously thought. Despite initial indications, clinical trials on the use of NSAIDs in already-diagnosed AD patients were found to be ineffective at slowing disease progression, and in some cases, even worsened clinical outcomes (6, 7). These contradictory findings have prompted the field to reexamine established hypotheses on the role of neuroinflammation in AD, which is now believed to be a dynamic and phase-dependent process (8, 9). During early, prodromal disease stages, neuroinflammation is likely a pathological accelerant, the effects of which can be mitigated by chronic NSAID use (9, 10). In contrast, neuroinflammation during late disease stages is likely associated with clearance of neural debris and Aβ plaques by phagocytic macrophages, and tissue resolution (8). Inhibiting these protective mechanisms in symptomatic patients with substantial neurodegeneration and established neuropathologies would likely have little benefit. As a result, understanding the earliest cellular processes that drive neuroinflammation during AD will be crucial in establishing therapeutic strategies aimed at derailing the disease trajectory, before the brain is affected beyond rescue.

Prior to the formation of extracellular plaques and tau neurofibrillary tangles (NFT), Aβ peptides and oligomers appear to accumulate within neurons of disease-vulnerable brain regions (11–15). This soluble pool of intraneuronal Aβ (iAβ) also increases in an age-dependent manner within the entorhinal cortex, a brain region regarded as the origin of AD neuropathological spread (13, 15). Despite the fact that Aβ oligomers represent the most toxic amyloid species within the brain (16–20), the effects of progressive iAβ build-up have scarcely been studied, and information on how this soluble pool may influence AD susceptibility is lacking.

Studies in several transgenic animal models of AD have consistently demonstrated that iAβ accumulation in the absence of plaque and tau pathologies is sufficient to produce synaptic abnormalities (21), long-term potentiation (LTP) impairment (21–24), and cognitive deficits (25–31), suggesting that the earliest

Significance

This work provides evidence that soluble and oligomeric amyloid protein stokes neuronal inflammation during the earliest stages of Alzheimer's disease. Identifying neuron-derived factors that engage the brain's immune system will provide insight into how vulnerable neurons might interact with other immune cells to propagate cytotoxic signaling cascades and cellular dysfunction during disease development.

Author contributions: L.A.W., S.D.C., and A.C.C. designed research; L.A.W., S.D.C., Z.M., J.C.M., and J.L. performed research; Z.M., J.L., W.L.K., and T.F. contributed new reagents/analytic tools; L.A.W., S.D.C., and J.C.M. analyzed data; and L.A.W., S.D.C., and A.C.C. wrote the paper.

The authors declare no competing interest.

This article is a PNAS Direct Submission.

[1]To whom correspondence may be addressed. Email: claudio.cuello@mcgill.ca.

This article contains supporting information online at https://www.pnas.org/lookup/suppl/doi:10.1073/pnas.1914593117/-/DCSupplemental.

First published March 6, 2020.

toxic effects of Aβ may in fact begin intraneuronally. Our laboratory and others have also shown that proinflammatory cytokines and chemokines become up-regulated within the brains of these animals months before initial plaque deposition and in the absence of cell loss (22, 32–38).

Despite the fact that Aβ accumulation is restricted to the intracellular space during this preplaque phase, the root cause of the corresponding neuroinflammatory response has yet to be identified. We therefore hypothesized that the Aβ-burdened neuron represents a primary proinflammatory agent during the earliest stages of the amyloid pathology, independent of extracellular plaques and cell death.

Using the McGill-R-Thy1-APP transgenic rat, which expresses the mutated human *amyloid precursor protein* (*APP*) gene, we extracted Aβ-burdened hippocampal neurons by laser-capture microdissection (LCM) and analyzed the effects of iAβ build-up on neuronal inflammatory gene expression. We demonstrate that key inflammatory mediators are up-regulated by neurons in preplaque APP transgenic rats, both at the transcript and protein levels, and that this inflammatory signal correlates with the localized recruitment of activated microglia. We also propose that a similar neuron-specific response may precede extracellular plaque deposition and pathological NFT formation within the human brain. Our findings suggest that progressive iAβ build-up unleashes a neuron-driven inflammatory process, triggering complex neuroimmune interactions at the outset of the AD neuropathological cascade.

Results

Aβ-Burdened Neurons Are Inflamed in Preplaque APP Transgenic Rats. To determine the effects of iAβ accumulation on neuronal inflammatory gene expression, neurons were extracted from the hippocampus of 5-mo-old wild-type (WT) and preplaque APP transgenic (Tg) rats by LCM and subjected to qRT-PCR. At 5 mo of age, the McGill-R-Thy1-APP rat exhibits significant accumulation of iAβ peptides and oligomers in the subiculum, CA1, CA3, and all cortical layers, as revealed by McSA1- and NU-1–immunolabeling, respectively (Fig. 1). Extracellular plaques are not observed in this animal model until 9 mo of age (30).

The pyramidal layer of the subiculum and CA1 was precisely excised by LCM to produce neuron-enriched histological samples with minimal glial contamination (Fig. 2*A* and *SI Appendix*, Fig. S1). When analyzed by qRT-PCR, levels of neuron-specific *MAP2* and *TUBB3* were found to be 3.3- and 2.1-fold higher, respectively, in our microdissected samples compared with whole-brain homogenate, validating that we had in fact obtained an enriched sample of neuron-derived mRNA (*SI Appendix*, Fig. S1*C*).

Microdissected neurons were then subjected to qRT-PCR using the RT^2 Cytokine and Chemokine Profiler PCR Array to measure differential expression of 84 transcripts commonly involved in inflammation and tissue resolution (*SI Appendix*, Table S1). Following quantitative analyses, we found a statistically significant increase in the expression of several chemotactic factors in Aβ-burdened neurons, including *CCL2* (*chemokine ligand 2*), *CCL3* (*chemokine ligand 3*), and *CSF-1* (*colony stimulating factor-1*) (Fig. 2*B*). We also detected a statistically significant decrease in the neuronal expression of *Cd70* and *IL-12α* (*interleukin-12 subunit alpha*) in these same Tg animals.

Next, to assess whether these inflammatory transcripts were similarly altered at the protein level, we performed neuron-specific fluorescence quantification following brain tissue double-immunolabeling. Using a fluorophore-conjugated antibody against NeuN, a highly specific marker for mature neurons, we quantified the fluorescence intensity of immunolabeled-cytokines exclusively within NeuN-immunoreactive (IR) cell bodies (*SI Appendix*, Fig. S2*A*). Consistent with our previous results, we found a statistically significant increase in neuronal CCL2 and CCL3 in the subiculum, as well as an increase in neuronal CCL2 in CA1 of our preplaque Tg rats; CCL3 signal intensity was unchanged in this region (Fig. 3).

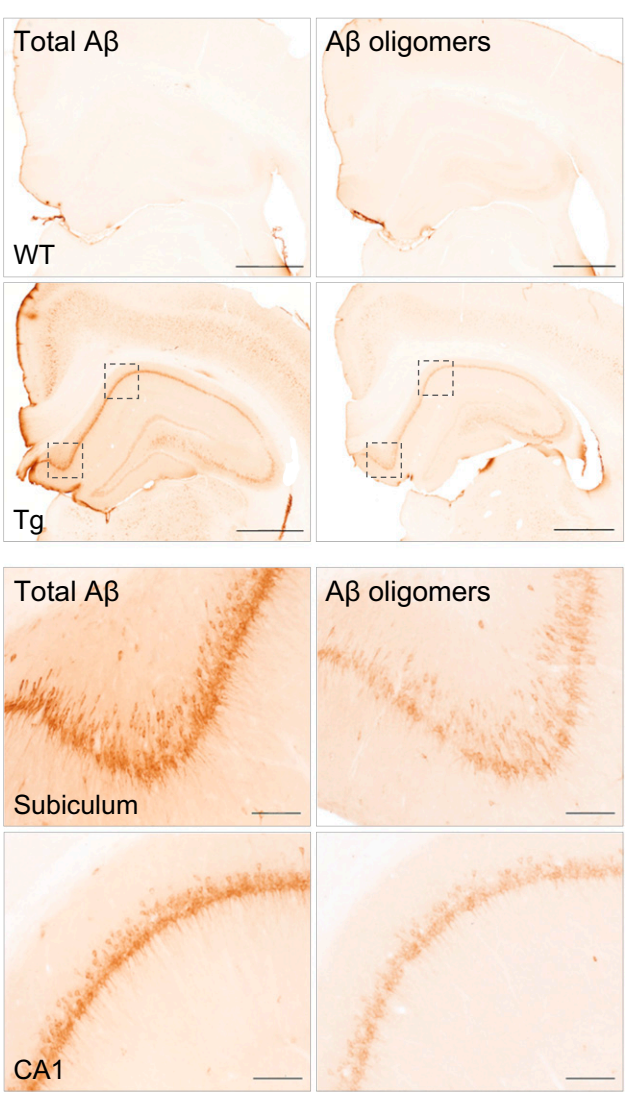

Fig. 1. Aβ peptides and oligomers accumulate within neurons of 5-mo-old McGill-R-Thy1-APP rats. At 5 mo of age, the McGill-R-Thy1-APP rat exhibits substantial iAβ accumulation without extracellular plaque deposition. (*A*) Neuronal Aβ peptides were detected throughout the hippocampus and cortex of preplaque Tg rats using the monoclonal McSA1 antibody. Oligomeric iAβ was also observed in the subiculum, CA1, CA3, and cortical layer V, as revealed by neuronal NU-1–IR. Brain tissue from WT animals was completely devoid of McSA1- and NU-1-immunolabeling. (Scale bars, 1 mm.) (*B*) High-magnification micrographs revealed the neuronal accumulation of Aβ peptides and oligomers in regions targeted by LCM. (Scale bars, 100 μm.)

Gene-expression analysis of microdissected neurons revealed an interesting trend in the expression of *IL-6* (*interleukin-6*): While neuronal *IL-6* was largely undetectable or detected at extremely low levels in most animals, four Tg rats exhibited very high expression levels compared with the control group. This suggested that the amount of tissue isolated by LCM may not have reached the critical mass necessary to reliably detect *IL-6* in all samples. Therefore, we decided to measure the relative protein expression of neuronal IL-6 by immunohistochemistry (IHC) in WT and Tg rats. Following fluorescence quantification, we did in fact find a statistically significant increase in neuronal IL-6 in the subiculum and CA1 of these preplaque Tg rats (Fig. 3).

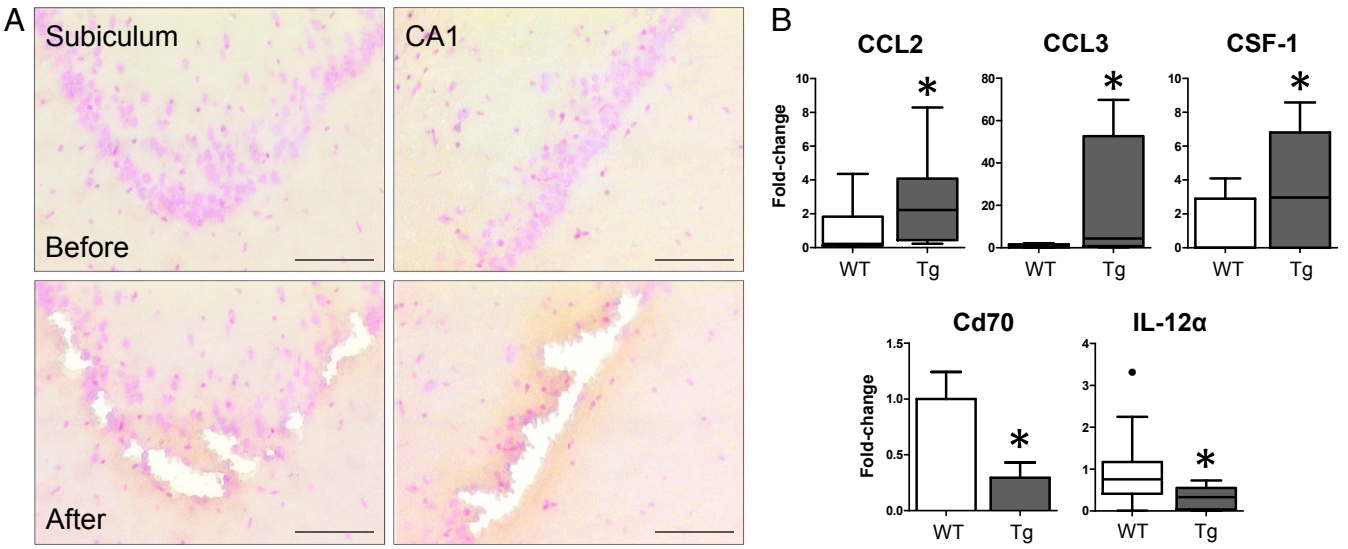

Fig. 2. Inflammatory gene-expression profile of Aβ-burdened neurons. (*A*) Tissue sections were stained with Cresyl violet to identify and differentiate neuronal and glial cells within the hippocampus of 5-mo-old rats. Neurons within the subiculum and CA1 were precisely excised by LCM to produce neuron-enriched histological samples. (Scale bar, 100 μm.) (*B*) Gene-expression analyses revealed a statistically significant increase in the expression of *CCL2*, *CCL3*, and *CSF-1*, as well as a decrease in the expression of *Cd70* and *IL-12α* in Aβ-burdened neurons extracted from preplaque Tg rats ($n = 10$ per genotype; $^*P < 0.05$).

Activated Microglia Are Recruited toward Inflamed Aβ-Burdened Neurons. We have previously observed that microglia become recruited toward hippocampal neurons in APP Tg mice (37) and rats (33, 38). Here, we hypothesized that activated microglia would become recruited toward the hippocampal pyramidal layer, even in the absence of extracellular plaques, in response to proinflammatory mediators produced by Aβ-burdened neurons. We therefore measured the number of microglia in proximity or in direct contact with hippocampal neurons in 5-mo-old WT and preplaque Tg rats. Indeed, we found a statistically significant increase in the number of Iba1-IR cells within 50 μm of the subiculum and CA1 of our Tg animals (Fig. 4*A*). This appeared to be a localized response, since the total number of microglial cells, as well as the total percent-area of Iba1-IR was found to be unchanged in the regions extending beyond the pyramidal layer (stratum oriens and stratum radiatum).

In response to an inflammatory stimulus, microglia undergo morphological changes that reflect a shift in their activation state. When adopting a "reactive" phenotype, microglia exhibit an increase in cell-body size and retraction of their processes, previously defined as an intermediate activation state (37, 39). This change in morphology can be measured by calculating the microglia dimensional ratio (DR) (*SI Appendix*, Fig. S2*B*), whereby an increase in DR is indicative of a shift toward a proinflammatory phenotype. Quantitative analysis revealed that microglia within the hippocampus of preplaque Tg rats did in fact exhibit an increase in DR compared with controls (Fig. 4*A*).

We also performed Pearson correlation coefficient analyses to determine if there was a relationship between neuronal cytokine expression and microglial reactivity. We found that levels of neuronal CCL2, as measured by quantitative fluorescent IHC, were positively correlated with the number of Iba1-IR cells in close proximity with the pyramidal layer of the hippocampus (Fig. 4*B*). Levels of neuronal IL-6 were also positively correlated with microglia DR, and thus the extent of microglial activation. Interestingly, this same linear relationship was not supported when neuronal CCL2 was correlated with microglia DR, or when neuronal IL-6 was correlated with microglial recruitment ($P > 0.05$). These findings indicate that, in this model, neuronal expression of chemotactic CCL2 is more closely related to microglial recruitment, while that of proinflammatory IL-6 is more closely related to microglial activation.

Neuron-Derived Inflammatory Factors Are Not Detected in Glia during the Preplaque Phase of the Aβ Pathology in APP Tg Rats. To assess the cell-specific expression of inflammatory factors found to be up-regulated in Aβ-burdened neurons, we performed double-immunolabeling of brain tissue from preplaque Tg rats using antibodies directed against microglia- and astrocyte-specific cell markers, Iba1 and GFAP, and inflammatory cytokines, CCL2, CCL3, and IL-6 (Fig. 5 *A* and *B*). No significant colocalization was observed between either glial cell-marker and any of the inflammatory molecules. Neurons were easily identifiable based on their intracellular cytokine immunolabeling, while glia could not be visualized without the use of their cell-specific markers. These results confirm that the up-regulation of CCL2, CCL3, and IL-6 likely represents a neuron-derived inflammatory signal, at least during the earliest stages of the Aβ pathology.

To corroborate our findings from gene expression and IHC analyses, we performed single-molecule RNA FISH, revealing the cell-specific localization of CCL2 transcripts in the hippocampus of 5-mo-old WT and Tg rats (Fig. 5*C*). Fluorophore-conjugated probes directed against GAPDH were used as a comparative positive control. Hippocampal neurons displayed stronger fluorescence-intensity associated with CCL2 mRNA compared with neighboring glial cells, both in WT and Tg animals; however, this difference in cell-specific expression appeared to be more pronounced in Tg rats. This observation not only confirms that neurons do in fact express appreciable levels of CCL2 mRNA under physiological conditions, but also that, in the context of iAβ pathology, neurons rather than glia produce a potent chemotactic signal through the up-regulation of *CCL2* transcription.

Lower Levels of iAβ Are Associated with Milder Inflammation in Young APP Tg Rats. At 5 mo of age, the McGill-R-Thy1-APP rat displays a robust neuron-specific inflammatory reaction and a corresponding microglial response. Given that this animal model exhibits progressive amyloid accumulation with age, we hypothesized that increasing levels of intracellular Aβ would amplify neuronal proinflammatory signaling and intensify the resulting immune response within the brain. Conversely, we were interested in whether those inflammatory processes observed in 5-mo-old Tg

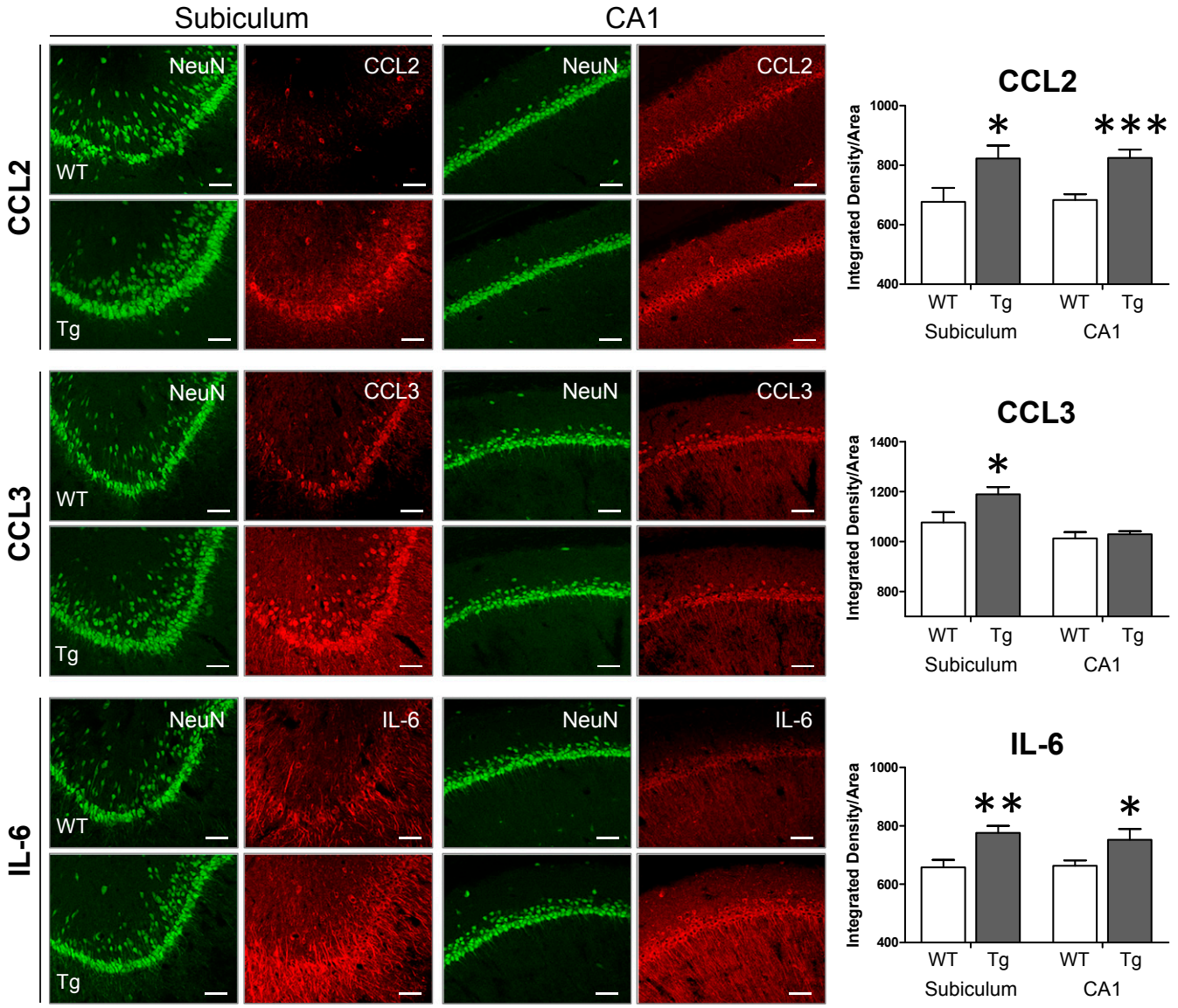

Fig. 3. Chemotactic and proinflammatory factors are up-regulated in hippocampal neurons of preplaque Tg rats. Double-immunolabeling followed by neuron-specific fluorescence quantification revealed a statistically significant increase in neuronal CCL2 and IL-6 within the subiculum and CA1 of 5-mo-old Tg rats compared with WT animals. Neuronal CCL3 was also more abundant within the subiculum ($n = 8$ per genotype; $^{*}P < 0.05$; $^{**}P < 0.01$; $^{***}P < 0.001$). (Scale bars, 50 μm.)

rats would be present in even younger animals harboring lower levels of brain Aβ. Employing similar analyses from previous experiments, we evaluated different aspects of neuroinflammation in 2-mo-old Tg rats. At this very early stage of the preplaque pathology, intracellular Aβ is detectable by McSA1 immunolabeling; however, iAβ levels are significantly lower in 2- compared to 5-mo-old rats, as measured by quantitative immunoenzymatic histochemistry (Fig. 6*A* and *SI Appendix*, Fig. S2*C*).

Having established a lower iAβ-load in these young Tg animals, we assessed whether changes in the neuronal expression of IL-6 could also be detected at 2 mo of age. Following neuron-specific fluorescence quantification, levels of IL-6 were found to be up-regulated within the subiculum, but unchanged in CA1 of 2-mo-old Tg rats when compared with controls (Fig. 6*B*). Microglial cells were also normally distributed throughout the hippocampus, as the number of neuron-proximal microglia in the subiculum and CA1 were similar between the two groups (Fig. 6*C*).

Our results show that, during the initial stage of the amyloid pathology, iAβ levels are sufficient to provoke the neuronal expression of cytotoxic IL-6 in certain disease-vulnerable brain regions, but not sufficient to induce microglial migration. Thus, it is likely that iAβ levels must reach a biological threshold to induce a neuron-driven inflammatory cascade.

Expression of CCL2 in the Human Medial Temporal Lobe Shifts from Neurons to Glia with Advancing Aβ Pathology. Our findings in an AD Tg rat model indicated that Aβ-burdened neurons, rather than glia, produce potent inflammatory mediators well before initial plaque deposition. Although the McGill-R-Thy1-APP rat is a valuable model for understanding the inflammatory effects that are specific to iAβ, it does not fully reflect the neuropathological environment of the human central nervous system (CNS). Given that progressive iAβ accumulation has also been observed in the human brain (11–15, 40), we posited that Aβ-burdened neurons may produce a similar, plaque-independent inflammatory signal within the human entorhinal cortex and

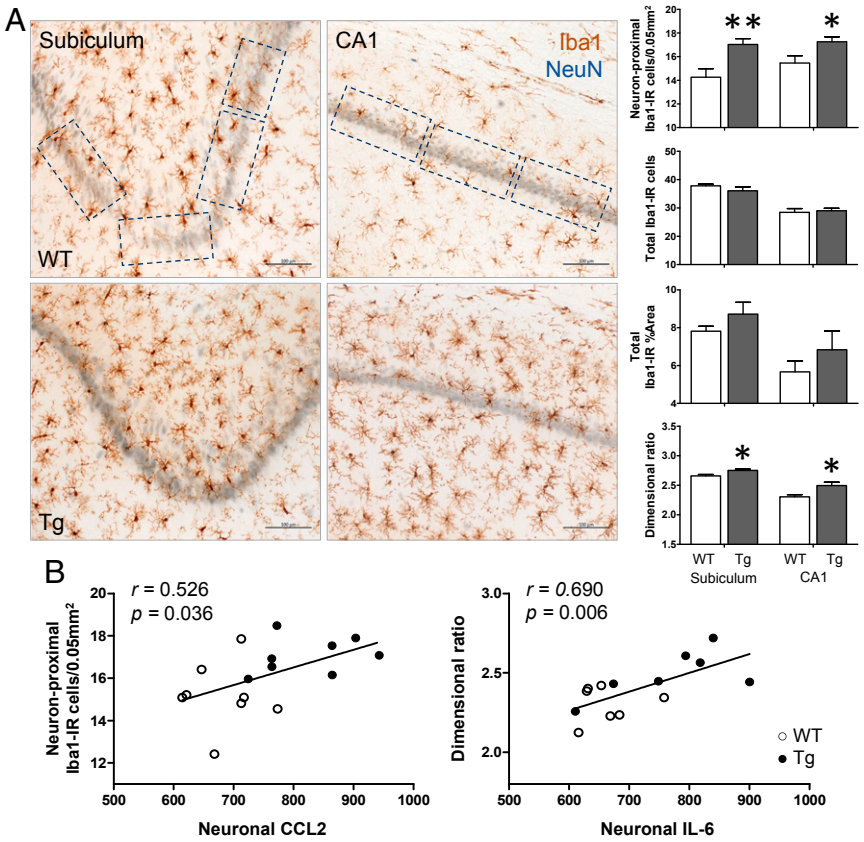

Fig. 4. Microglia are recruited toward Aβ-burdened neurons and exhibit activated morphology in the absence of extracellular plaques. (*A*) To measure changes in microglial mobilization in the context of iAβ pathology, the number of Iba1-immunopositive cells (brown) within 50 μm of the subiculum and CA1 (indicated with boxes) were manually counted. NeuN was used as a marker of mature neurons (blue). Statistical analysis revealed a significant increase in the number of Iba1-IR cells in proximity or in direct contact with Aβ-burdened neurons in 5-mo-old Tg rats. In contrast, the total number of microglia within the hippocampus, as well as the total Iba1-IR percent-area were comparable between WT and Tg animals. Microglia from Tg rats also displayed morphological changes consistent with a proinflammatory phenotype, as revealed by an increase in dimensional ratio ($n = 8$ per genotype; $^{*}P < 0.05$; $^{**}P < 0.01$). (Scale bars, 100 μm.) (*B*) Pearson correlation analysis revealed that the number of neuron-proximal microglia was positively correlated with the abundance of neuronal CCL2 protein in CA1 of the hippocampus. In addition, microglia dimensional ratio was positively correlated with levels of neuronal IL-6 ($n = 7$ to 8 per genotype).

hippocampus. We therefore compared the cell-specific expression of CCL2 in the human medial temporal lobe of subjects with and without extracellular plaques. For these purposes, we analyzed a collection of extremely well-preserved brain tissue obtained with short postmortem delay (2 to 4 h for all cases) and processed by perfusion-fixation. Such high-quality postmortem material is ideal for detecting subtle differences in the cell-specific expression of cytokines in the context of an evolving Aβ pathology.

All subjects analyzed were between 66 and 77 y of age at the time of death. Control subjects died of causes unrelated to neurological disease and did not exhibit cognitive or movement alterations. Minimal AT8-IR tau was restricted to the entorhinal cortex (Braak stages 0–I). TDP-43 pathology in the form of neuronal cytoplasmic inclusions and dystrophic neurites was only observed in one subject with diagnosed AD. None of the cases exhibited motor neuron damage or Lewy body pathology.

First, we used the monoclonal antibody, McSA1, targeting the N-terminal amino acids 1 to 12 of human Aβ to evaluate the extent of Aβ accumulation in postmortem brains of nondemented and AD subjects. We have previously shown by peptide preadsorption and superresolution structured illumination microscopy that McSA1 is highly specific for human Aβ and does not cross-react with the APP holoprotein or its cleavage products (15, 29, 41). In control cases, we found that all neurons exhibited substantial iAβ material (Fig. 7*A*). One subject with diagnosed AD displayed advanced plaque deposition throughout layers III–VI of the entorhinal cortex and all regions of the hippocampus, while McSA1-IR neurons were sparse and difficult to visualize, likely due to extensive plaque pathology and advanced neurodegeneration.

Next, we used the same anti-CCL2 monoclonal antibody utilized for animal experiments to analyze the cell-specific expression of CCL2 in these samples. In control subjects devoid of extracellular plaques, CCL2-IR was observed in all neurons of the entorhinal cortex, subiculum, and CA1 (Fig. 7 *B* and *C*). Adjacent glia could also be detected but exhibited only faint immunolabeling (Fig. 7*D*).

Interestingly, glia displayed more intense CCL2-IR in subjects with extracellular plaques. While Aβ-burdened neurons appeared to remain the predominant source of CCL2 within these brain regions, a progressive shift toward increased glial CCL2 became apparent as insoluble plaque pathology developed.

The cell-specific expression of CCL2 within the AD brain with abundant plaques was notably different from that observed in control samples: While CCL2-IR neurons could still be clearly visualized, CCL2-IR became much more pronounced throughout glial cell bodies and extending processes (Fig. 7*D*). Our findings in the human brain reflect those obtained from our AD-like Tg rat model: In the absence of extracellular plaques, Aβ-burdened neurons represent the predominant source of CCL2

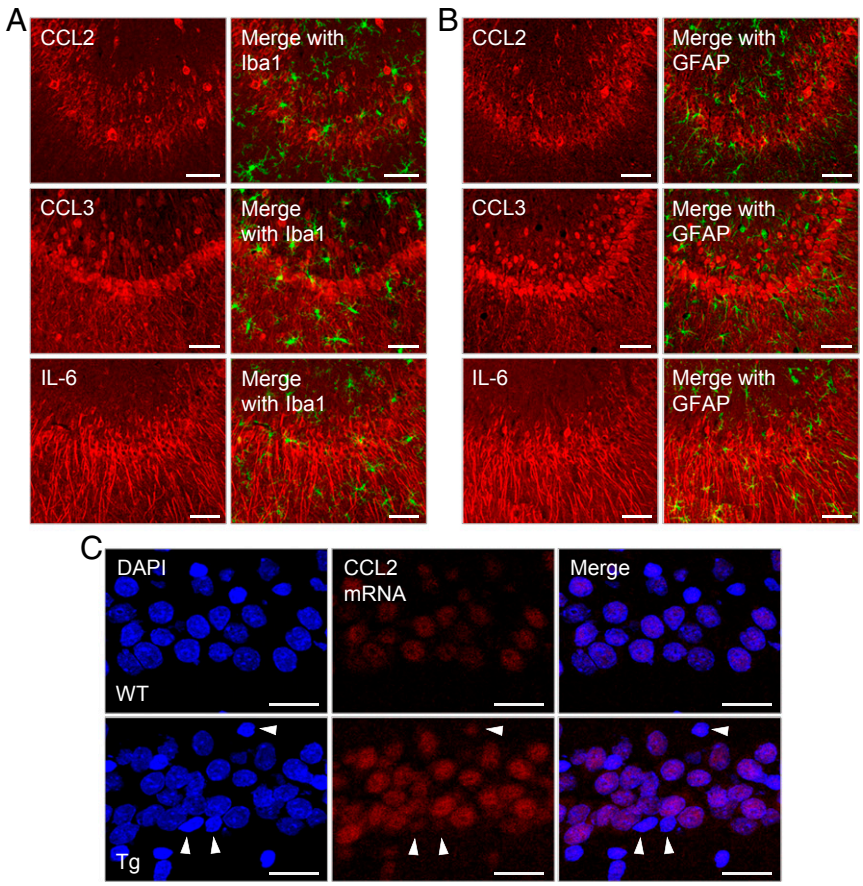

Fig. 5. Inflammatory mediators are up-regulated in Aβ-burdened neurons of preplaque Tg rats, but not in neighboring glial cells. Inflammatory mediators found to be up-regulated in Aβ-burdened neurons were probed by IHC (red), along with cell-specific markers, Iba1 (*A*) and GFAP (*B*), to identify brain macrophages and astrocytes, respectively (green). In 5-mo-old Tg animals, most cytokine-IR was observed within neurons of the hippocampus. No colocalization was found between glial cells and any of the inflammatory factors analyzed at this early pathological stage. (Scale bars, 50 μm.) (*C*) Using fluorescent oligonucleotide probes (red), CCL2 transcripts appeared to be more abundant within neurons of the hippocampus compared with neighboring glial cells (indicated by white arrowheads), which were distinguishable based on their characteristic DAPI staining (blue). (Scale bars, 20 μm.)

within AD-vulnerable brain regions, while advanced plaque deposition and neurodegeneration is likely associated with a shift toward a glial immune response. These observations reinforce the duality of the role of neuroinflammation in early versus late pathological stages of AD.

Discussion

In the present study, we show that neurons participate in Aβ-driven neuroinflammation during the earliest stages of the amyloid pathology. By targeting and extracting specific populations of hippocampal neurons from preplaque APP Tg rats, we demonstrate that iAβ accumulation is sufficient to induce neuronal inflammatory signaling and microglial recruitment, months before initial plaque deposition and independent of cell death. Quantitative gene expression and IHC analyses revealed that these neurons generate a variety of potent chemotactic and proinflammatory molecules—including CCL2, CCL3, CSF-1, and IL-6—most of which are only detected in low quantities in microglia and astroglia at this early time-point.

With the recent discovery of immune-related genetic loci associated with increased AD risk (42, 43), research efforts have shifted toward understanding how microglia initiate and propagate neuroinflammation during AD with little regard for other major cell types within the brain. Experimental measures of neuroinflammation are most often attributed to changes in microglial activation, even though analytes assessed in whole-tissue samples are derived from a composite of cell-types, including neurons, astrocytes, oligodendrocytes, and components of the neurovascular unit. Although microglia are classically regarded as the primary immune cells within the CNS, they are not the sole effectors of neuroinflammation. As an example, astrocytes adopt a neurotoxic "A1" phenotype and lose critical neurotrophic functions following exposure to proinflammatory molecules and complement factors (44). Evidence also supports the potential role of oligodendrocytes in regulating immune responses in demyelinating diseases, such as multiple sclerosis, through the expression of cytokines and chemokines (45). Exposure of "eat me" molecules at the cell surface of neurons harboring toxic tau inclusions represents another mechanism by which nonmicroglial cells can stimulate the brain's immune system (46).

Previous attempts have been made to characterize the AD neuronal transcriptome from microdissected samples recovered from archival postmortem brain material; however, as a result of long-term tissue fixation and storage conditions, techniques commonly used to measure differential gene expression, such as microarrays, RNA-seq, and mass spectrometry, can only detect robust transcriptional changes. Consequently, it is unlikely that low-abundant inflammatory transcripts could be detected or quantified from only a few-hundred cells, as is typically reported (47–51). In the present study, we employed LCM to extract thousands of pyramidal neurons from disease-relevant brain regions from flash-frozen tissue, allowing us to produce an enriched sample of

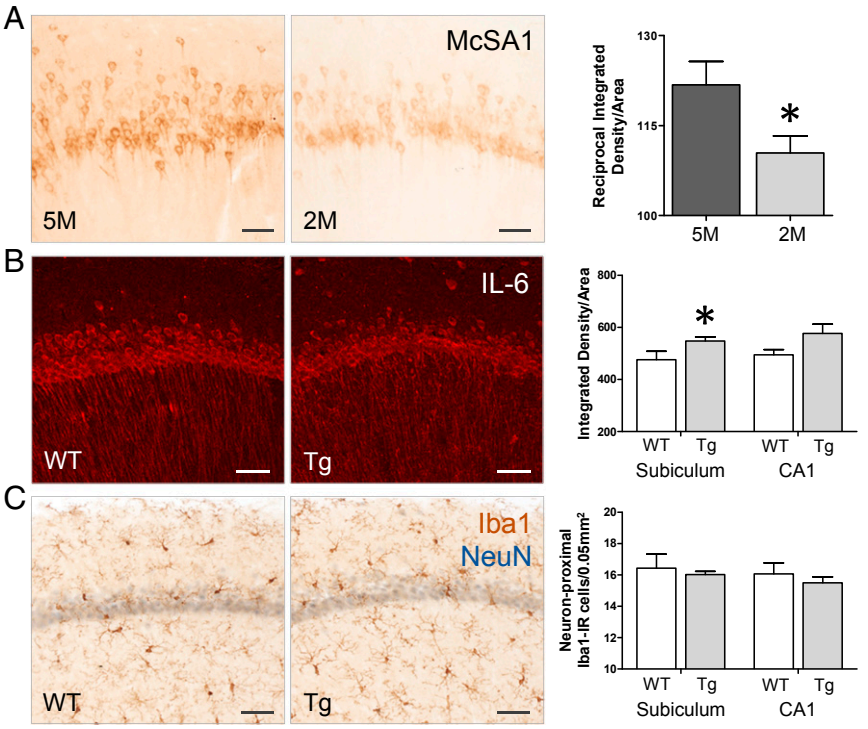

Fig. 6. Lower levels of iAβ are associated with milder inflammation in young preplaque Tg rats. (*A*) Compared with 5-mo-old Tg rats, levels of iAβ were significantly lower at 2 mo of age, as measured by neuronal McSA1-IR ($n = 7$ per age; $^*P < 0.05$). (Scale bars, 50 μm.) (*B*) Neuronal IL-6 was found to be increased in the subiculum of 2-mo-old Tg rats, as determined by Mann–Whitney *U* test; however, levels in CA1 were comparable between WT and Tg animals ($n = 6$ to 7 per genotype; $^*P < 0.05$). (Scale bars, 50 μm.) (*C*) Similarly, the number of neuron-proximal (blue) Iba1-immunopositive cells (brown) within the hippocampus of Tg rats was unchanged at 2 mo of age ($n = 6$ to 7 per genotype). (Scale bars, 50 μm.)

neurons bearing the highest quantity of intracellular Aβ. By performing target-specific amplification and quantitative gene-expression analysis using a PCR array specially designed to detect low-abundant inflammatory transcripts from low-yield samples, such as those produced by LCM, we successfully characterized the inflammatory profile of Aβ-burdened neurons, the results of which were validated by quantitative IHC and RNA FISH.

Each molecule up-regulated in Aβ-burdened neurons has also been shown to be expressed by neurons in the healthy and AD brain (52–55). In fact, several studies have demonstrated that levels of CCL2 and IL-6 are increased in the brains of patients with mild cognitive impairment (MCI) and AD (56–58), with one study suggesting that neurons exhibit the most pronounced increase in CCL2- and IL-6 when analyzed by IHC (54).

CCL2 in particular has been repeatedly implicated in early disease development. Although little is known about the preplaque neuroinflammatory environment, two independent studies have shown that CCL2 is increased in both brain and plasma of young, preplaque 3xTg mice with substantial iAβ accumulation (37, 59). Similarly, CCL2 has been found to be up-regulated in cerebrospinal fluid (CSF) and blood plasma of patients with MCI and mild AD (60–63). MCI patients with higher levels of CCL2 at baseline also exhibit faster rates of cognitive decline and shorter time-to-conversion to AD, suggesting that CCL2 signaling may be most relevant during early disease stages (64, 65). Similarly, increasing levels of CCL2 in patients with MCI and AD are associated with elevated levels of total-tau and phospho-tau in CSF, smaller medial temporal lobe volume, and lower cognitive memory scores (66–68). In the present study, IHC detection of CCL2 revealed that, in the absence of extracellular plaques and pathological tau, Aβ-burdened neurons represent the predominant source of CCL2 within the human medial temporal lobe. In the context of advancing plaque pathology and neurodegeneration, however, CCL2 expression is markedly increased in glial cells, indicating a shift in cell-specific responses. Our findings underscore the fact that different cell-types variably contribute to CNS inflammation during AD.

CCL3 and CSF-1 expression are also altered in the context of AD. For example, levels of CCL3 in plasma are elevated in patients with higher neocortical Aβ burden, as determined by positron emission tomography (69). CSF-1 and other components of the CSF-1 signaling pathway are similarly up-regulated in the postmortem AD brain (58). Additionally, CSF-1 potentiates the proinflammatory effects of Aβ in hippocampal organotypic cultures, enhancing the release of CCL3 and IL-6 (70).

Surprisingly, Aβ-burdened neurons from preplaque Tg rats exhibited decreased expression of IL-12α, which is one of two components of the proinflammatory IL-12 heterodimer. Reports on the expression of IL-12 in humans and Tg mouse models of AD are limited and contradictory. One study has demonstrated that levels of IL-12 are decreased in the CSF of patients with AD compared with age-matched controls (71), while others have reported that levels of IL-12 are unchanged (72). It has also been shown that brain IL-12 is increased in two different Tg mouse models of AD; however, it is important to note that these studies were performed using animals with advanced plaque deposition, and measurements were conducted on either the full IL-12 heterodimer or the IL-12β subunit. To that point, other investigations profiling iAβ-associated neuroinflammation have demonstrated that, before extracellular plaque deposition, levels of IL-12α and IL-12 are in fact decreased in the brains of young Tg mice (37, 73). These data are consistent with the findings from our preplaque Tg rat model.

Coincident with the emergence of iAβ-mediated inflammation, we found that microglia adopt an intermediately activated morphological phenotype and become recruited toward the pyramidal

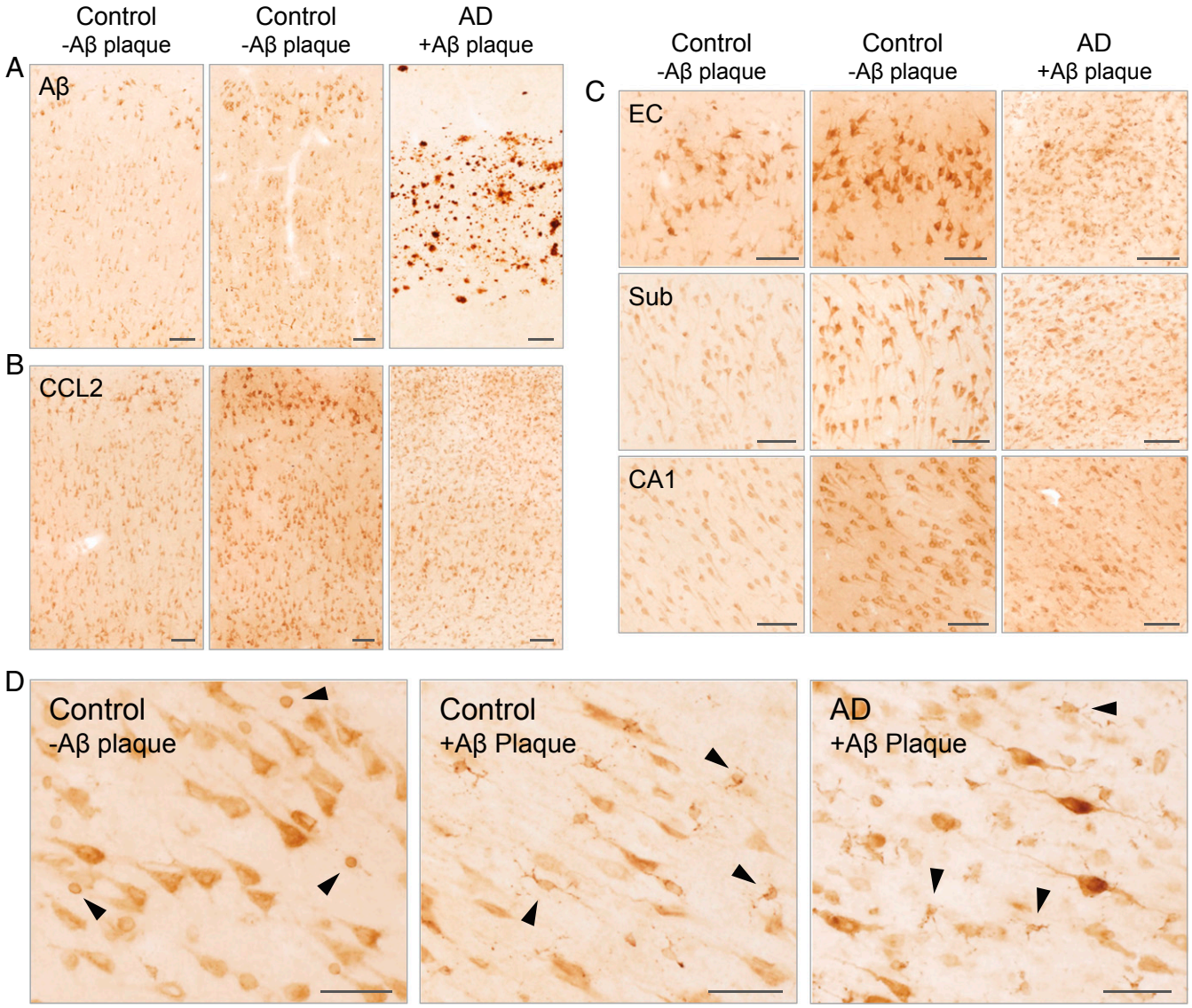

Fig. 7. Aβ-burdened neurons are the predominant source of CCL2 in the human brain in the absence of extracellular plaques and pathological tau. (*A*) All neurons within the entorhinal cortex of nondemented subjects exhibited substantial intracellular Aβ accumulation, as revealed by McSA1 immunolabeling. One case with diagnosed AD exhibited advanced extracellular plaque pathology throughout the entorhinal cortex and medial temporal lobe, while McSA1-IR neurons were sparse and difficult to visualize. (Scale bars, 100 μm.) (*B*) In nondemented subjects devoid of extracellular plaques, Aβ-burdened neurons exhibited strong CCL2-IR throughout the entorhinal cortex. In contrast, glia appeared to represent the major CCL2-immunpositive cell-type within the AD brain. (Scale bars, 100 μm.) (*C*) The cell-specific expression of CCL2 was consistent throughout all regions of the medial temporal lobe, including the subiculum (Sub) and region CA1. (Scale bars, 100 μm.) (*D*) High-magnification micrographs revealed differential expression of CCL2 as a function of progressive Aβ pathology. In the absence of extracellular plaques, Aβ-burdened neurons appear to be the predominant source of CCL2 within the human medial temporal lobe, while established plaque pathology is associated with a progressive shift toward increased glial CCL2 expression (black arrowheads indicate CCL2-IR microglia). (Scale bars, 50 μm.)

layer of the hippocampus. Under physiological conditions, "resting" microglia continuously patrol and survey their microenvironment through rapid extension and retraction of their processes (74, 75). In addition to these dynamic structural changes, microglia express a variety of surface receptors, allowing them to sample the neurochemical byproducts of both homeostatic and damage-associated processes (76). Accordingly, we found that, in the absence of extracellular plaques, the neuronal expression of chemotactic CCL2 was positively correlated with the number of neuron-proximal microglial cells, whereas proinflammatory IL-6 was positively correlated with the extent of microglial activation.

Microglia are also crucial to the maintenance of neural networks, forming brief and frequent contacts with neuronal synapses to monitor and regulate firing activity (77). Interestingly, elevated levels of CCL3, which were also observed in Aβ-burdened neurons, produce aberrant neural firing patterns in vitro (78) and suppress synaptic transmission and behavioral performance in vivo (79). The consequences of sustained neuronal inflammation and excessive neuroglial interactions may explain many of the functional deficits observed in preplaque Tg animal models, including our own: Even in the absence of extracellular plaques, the McGill-R-Thy1-APP rat displays substantial LTP impairment and cognitive dysfunction (24, 29, 30, 80, 81).

The combined effects of chronic inflammatory signaling by Aβ-burdened neurons and aberrant neuroglial contacts may contribute to dysregulated synaptic firing and early neuronal

dysfunction. However, it is also possible that iAβ-mediated cellular stress might precipitate the release of neuron-derived cues that mark an increased demand for glial trophic support. The nature of these neuroglial interactions in our preplaque Tg rat model is, at present, unclear; however, they are likely time- and context-dependent. For example, CCL2 knockout or inhibition minimizes plaque pathology, diminishes inflammatory gene expression, and recovers cognitive performance in an AD Tg mouse model, but may have converse effects in otherwise WT animals (82, 83). In an experimental animal model of encephalitis, neuron-derived CCL2 promotes the recruitment of phagocytic macrophages and synaptic engulfment, resulting in significant motor deficits (84). In contrast, microglial contact at specialized neuronal somatic junctions likely protects against hypoxic injury, limiting lesion-size and cognitive impairment following stroke-induced ischemia (85). Similarly, it is unknown whether preplaque neuronal inflammatory signaling is harmful in aggravating cytotoxic damage, or beneficial in engaging immune trophic support during early stages of AD. Understanding how these complex neuroglial interactions influence the brain's immune system at varying stages of disease will ultimately inform on which molecular pathways may be most amenable to early therapeutic intervention.

Although the amyloid plaque represents a potent immunological structure within the brain, comprising an agglomerate of insoluble proteins, toxic cytokines, and complement factors, it is well-established that plaque-load is a poor correlate of cognitive decline, cell loss, and NFT density in disease-vulnerable brain regions (20, 86–91). Rather, compared with amyloid plaques, increasing levels of soluble Aβ are a better predictor of synaptic dysfunction, cognitive deficits, and pathological tau when analyzed in the postmortem AD brain (16, 18–20). We propose that the incremental build-up of soluble and oligomeric iAβ may provoke a neuron-specific immune reaction, setting off a neuroinflammatory cascade at the earliest stages of AD.

In sum, our findings reinforce the idea that the neuroinflammatory environment within the AD brain is complex, dynamic, and phase-dependent (8). We provide definitive evidence that the intracellular accumulation of Aβ is sufficient to trigger a neuron-derived inflammatory reaction, which is characterized by chemotactic signaling and mobilization of activated microglia toward the site of damage. Most importantly, we have shown that Aβ-burdened neurons act as "inflammatory agents" during the earliest stages of the amyloid pathology, and that this neuroinflammatory process is likely distinct from plaque-associated immune responses. Thus, the findings of our study have significant implications regarding the origin of the initial inflammatory reaction within the AD brain.

Materials and Methods

Animals and Brain Tissue Processing. McGill-R-Thy1-APP Tg rats express the human *APP* gene containing the Swedish and Indiana mutations under control of the murine Thy1.2 promoter. Male and female WT and homozygote Tg rats were housed in humidity- and temperature-controlled rooms under a 12-h light/dark cycle with access to food and water ad libidum. At 2 and 5 mo of age, rats were anesthetized with equithesin (pentobarbital based, 2.5 mL/kg, i.p. injection) followed by transcardiac perfusion with ice-cold 0.1 M phosphate buffer. All procedures were approved by the Animal Care Committee of McGill University and conform to the guidelines set out by the Canadian Council on Animal Care. Additional information on tissue processing can be found in *SI Appendix*.

Human Subjects and Brain Tissue Processing. Nondemented control and AD subjects were processed for autopsy in Saint Borbála Hospital, Department of Pathology, Tatabánya, Hungary. Informed consent was obtained for the use of brain tissue after death and for access to medical records for research purposes. Tissue was obtained and used in compliance with the 1964 Declaration of Helsinki and its amendments or comparable ethical standards, and all procedures were approved by the Regional and Institutional Committee of Science and Research Ethics of Scientific Council of Health [EET TUKEB 31443/2011/EKU (518/PI/11)].

Postmortem brain material was harvested and processed as previously described (15). Briefly, brains were removed 2 to 5 h postmortem and perfused via the internal carotid and vertebral arteries with physiological saline and fixative solution containing 4% PFA, 0.05% glutaraldehyde, and 0.2% picric acid. The medial temporal lobe was dissected and postfixed overnight in the same fixative solution without glutaraldehyde before being transferred to a sucrose solution, rendering optimal tissue preservation for microscopic analysis. Once received at McGill University, tissue blocks were cut into 40-μm-thick sections and stored in cryoprotectant at −20 °C.

Laser Capture Microdissection. Flash-frozen brain tissue from 5-mo-old WT and Tg rats was cut into 10-μm-thick sections using a Leica CM3050S cryostat. Tissue was thaw-mounted onto 1.0-mm PEN membrane-covered glass slides (MembraneSlide 1.0 PEN; Carl Zeiss), which were irradiated with UV light for 30 min prior to cryosectioning. Mounted tissue sections were stained with Cresyl violet, as described in *SI Appendix*.

The entire pyramidal layer of the subiculum and CA1 was microdissected from 40 tissue sections per animal using the PALM MicroBeam (Carl Zeiss). Neurons were identified based on their characteristic Cresyl violet staining: Neurons stained diffusely throughout the entire cell body, while glial cells exhibited darker staining exclusively within the nucleus. Microdissected neurons were pressure-catapulted into 200-μL PCR tubes with opaque adhesive cap (AdhesiveCap 200 Opaque; Carl Zeiss) using the following UV-laser settings: Cut energy, 75; cut focus, 70; auto-LPC dot-size, 12 (*SI Appendix*, Fig. S1*A*). mRNA extraction was performed immediately following LCM, as detailed in *SI Appendix*.

RT^2 Rat Cytokine and Chemokine Profiler PCR Array. To evaluate the inflammatory gene-expression profile of microdissected neurons by qRT-PCR, mRNA was converted to cDNA and subjected to primer-specific amplification using the RT^2 PreAMP cDNA Synthesis Kit and Pathway Primer Mix respectively (Qiagen). Amplified cDNA from each animal was then analyzed using the RT^2 Rat Cytokine and Chemokine Profiler PCR Array (PARN-150Z; Qiagen). The expression of 84 inflammatory genes was measured over 45 thermal cycles using the CFX Connect Real Time cycler (Bio-Rad Laboratories) with the recommended cycling conditions provided by Qiagen. The relative expression of each transcript was calculated using the $\Delta\Delta C_T$ method and standardized against five housekeeping genes. Three internal controls were also included to evaluate the presence of genomic DNA contamination and the efficiency of the reverse transcription and polymerase chain reactions. The relative expression of cell-specific markers found in microdissected samples was quantified as described in *SI Appendix*, Fig. S1*C* and Table S2.

Brightfield and Fluorescent IHC. Detailed experimental protocols describing antibody dilutions and incubation times for immunostaining of both rat and human brain tissue can be found in *SI Appendix*.

Single-Molecule RNA FISH. Flash-frozen brain tissue was cryosectioned into 10-μm-thick slices, thaw-mounted onto standard glass microscope slides and stored at −80 °C until processed for RNA FISH. Sections were transferred directly from storage to 4% PFA for 15 min at 4 °C, and then processed according to the protocol provided by LGC Biosearch Technologies for Stellaris RNA FISH, as described in *SI Appendix*. A mixture of 25 CAL610-conjugated oligonucleotide probes, each 20 nucleotides in length, targeting rat CCL2 mRNA were designed using the online Stellaris Probe Designer (NCBI Reference Sequence: NM_031530.1). Confocal imaging was completed within 30 h.

Microscopy and Image Analysis.

Quantifying fluorescence intensity of neuronal cytokines. For each cytokine measured, two tissue sections from WT and Tg rats were immunolabeled as described in *SI Appendix* and imaged by confocal microscopy. Acquisition settings were held constant for all images being compared by quantitative analysis. One image containing the entirety of the subiculum and four to five images centered on the pyramidal layer of CA1 were acquired as 6-μm *z*-stacks using a 20× objective and converted to maximum intensity projections using Zen 202 SP5 Black (Carl Zeiss).

To quantify fluorescence intensity of immunolabeled cytokines exclusively within neurons, confocal images were processed using ImageJ software (National Institutes of Health). The channel corresponding to NeuN (green) was converted to a binary image using "Triangle"-thresholding, and regions of interest (ROI) were defined as NeuN-immunopositive areas larger than 10 μm (*SI Appendix*, Fig. S2*A*). These ROI were then applied to the channel corresponding to the cytokine being measured (*SI Appendix*, Fig. S2*A*, red) and fluorescence intensity was quantified exclusively within those ROI.

Signal intensity of each image is expressed as the total ROI integrated density normalized by the total ROI area.

Quantifying microglial recruitment and activation. To identify neurons and microglia within the hippocampus of WT and Tg rats, two tissue sections per animal were immunolabeled with anti-NeuN and -Iba1 antibodies, as described in *SI Appendix*.

To measure microglial mobilization toward Aβ-burdened neurons, one image containing the entirety of the subiculum and four images centered along the pyramidal layer of CA1 were acquired as *z*-stacks using a 20× objective and processed using the "Extended Depth of Focus" function in Zen 2.3 Blue software (Carl Zeiss). Fixed-area boxes of varying sizes (0.01 to 0.02 mm^2) were manually centered on the pyramidal layer of the subiculum and CA1, encompassing Iba1-immunopositive cells within 50 μm of hippocampal neurons. The number of microglial cells was manually counted and expressed as a function of area (0.05 mm^2).

To assess the extent of microglial activation, double-fluorescent immunolabeling was performed using the same primary antibodies, and *z*-stack projections were acquired by confocal microscopy. To calculate microglia dimensional ratio, which represents cell body-size proportional to process-length, we first measured the total image-area occupied by Iba1-IR (*SI Appendix*, Fig. S2*B*). Images were then converted to binary and skeletonized to measure the total length of microglial processes. The dimensional ratio of each image was calculated from: (Iba1-IR area)/(Iba1-IR length).

Assessing cell-specific expression of CCL2 mRNA. Tissue sections from WT and Tg rats were subjected to RNA FISH as described above. Images centered along the pyramidal layer of CA1 were acquired as 5-μm *z*-stacks using a 63× objective with 1.5× zoom, and then converted to maximum-intensity projections.

Quantifying chromogen intensity of neuronal McSA1-IR. To quantify the neuronal accumulation of Aβ peptides, the relative intensity of neuronal McSA1-IR was quantified. Three images centered on CA1 were acquired using a 20× objective, converted to greyscale and variably thresholded using ImageJ software so pyramidal cells could be precisely delineated and manually selected as ROI (*SI Appendix*, Fig. S2*C*). The integrated density and area of all ROIs (i.e., CA1 pyramidal neurons) were measured and summated (Σ integrated density/Σ area) to produce one value representing the total signal intensity for each image. Chromagen intensity was then quantified using the reciprocal intensity (*r*) method (15), whereby higher "*r*" values are associated with more intense chromogen staining, and thus higher protein levels. Tissue sections were processed simultaneously to maintain identical immunolabeling and staining conditions.

Statistical Analysis. Comparisons were performed between genotypes within each brain region analyzed. Independent sample *t*-tests were performed for all parametric analyses. When the *F*-statistic was significant, a Welch's *t* test was applied. Values more than two SDs from the mean were considered outliers and excluded. Mann–Whitney *U* nonparametric tests were performed when normal distribution could not be assumed, as determined by the Shapiro–Wilk normality test. Values larger than three-times the interquartile range were considered outliers and excluded.

Data subjected to parametric analysis are displayed in column bar graphs, where error bars represent the mean ± SEM. Unless otherwise specific, data subjected to nonparametric analyses are displayed in box-and-whiskers plots with the Tukey method, where the median is represented by the horizontal line and the 25th and 75th percentiles extend from the extremes of the box.

To assess the relationship between neuronal cytokine expression and microglial reactivity, Pearson correlation coefficient (*r*) was measured.

The sample size *n* for each experiment represents the number of animals tested. Each data point represents the average value of all technical replicates per animal. The final sample size is represented in all figures. Significance was set at $P < 0.05$ for all statistical tests.

Data Availability. Additional information on the data presented is available upon request.

ACKNOWLEDGMENTS. We thank Dr. Alfredo Ribeiro-da-Silva for allowing us to use the Axio Imager M2 widefield microscope and for his guidance and assistance in acquiring the images presented; and the McGill University Advanced BioImaging Facility for their help with laser-capture microdissection and confocal microscopy. The A.C.C. laboratory is grateful for the unrestricted support received from Dr. Alan Frosst, the Frosst family, and Merck Canada. This research is supported by the Canadian Institutes of Health Research Project Grant PJT-364544 (to A.C.C.) and 2017-1.2.1-NKP-2017-00002 (to the Human Brain Research Laboratory). L.A.W. is the recipient of a Doctoral Training Fellowship from the Fonds de recherche du Québec–Santé. S.D.C. is the holder of the Charles E. Frosst/Merck Research Associate position. J.C.M. was the recipient of a Rotary Foundation Global Grant Scholarship. A.C.C. is the holder of the McGill University Charles E. Frosst/Merck Chair in Pharmacology and is a member of the Canadian Consortium on Neurodegeneration in Aging.

1. H. Akiyama, Inflammatory response in Alzheimer's disease. *Tohoku J. Exp. Med.* **174**, 295–303 (1994).
2. P. Eikelenboom, F. C. Stam, Immunoglobulins and complement factors in senile plaques. An immunoperoxidase study. *Acta Neuropathol.* **57**, 239–242 (1982).
3. P. L. McGeer, S. Itagaki, E. G. McGeer, Expression of the histocompatibility glycoprotein HLA-DR in neurological disease. *Acta Neuropathol.* **76**, 550–557 (1988).
4. P. L. McGeer, S. Itagaki, H. Tago, E. G. McGeer, Reactive microglia in patients with senile dementia of the Alzheimer type are positive for the histocompatibility glycoprotein HLA-DR. *Neurosci. Lett.* **79**, 195–200 (1987).
5. P. L. McGeer, E. G. McGeer, The amyloid cascade-inflammatory hypothesis of Alzheimer disease: Implications for therapy. *Acta Neuropathol.* **126**, 479–497 (2013).
6. ADAPT-FS Research Group, Follow-up evaluation of cognitive function in the randomized Alzheimer's disease anti-inflammatory prevention trial and its follow-up study. *Alzheimers Dement* **11**, 216–225.e1 (2015).
7. D. Jaturapatporn, M. G. Isaac, J. McCleery, N. Tabet, Aspirin, steroidal and non-steroidal anti-inflammatory drugs for the treatment of Alzheimer's disease. *Cochrane Database Syst. Rev.*, CD006378 (2012).
8. A. C. Cuello, Early and late CNS inflammation in Alzheimer's disease: Two extremes of a continuum? *Trends Pharmacol. Sci.* **38**, 956–966 (2017).
9. J. Rogers, Principles for central nervous system inflammation research: A call for a consortium approach. *Alzheimers Dement.* **14**, 1553–1559 (2018).
10. J. C. Breitner *et al.*; ADAPT Research Group, Extended results of the Alzheimer's disease anti-inflammatory prevention trial. *Alzheimers Dement.* **7**, 402–411 (2011).
11. M. R. D'Andrea, R. G. Nagele, H. Y. Wang, D. H. Lee, Consistent immunohistochemical detection of intracellular beta-amyloid42 in pyramidal neurons of Alzheimer's disease entorhinal cortex. *Neurosci. Lett.* **333**, 163–166 (2002).
12. M. R. D'Andrea, R. G. Nagele, H. Y. Wang, P. A. Peterson, D. H. Lee, Evidence that neurones accumulating amyloid can undergo lysis to form amyloid plaques in Alzheimer's disease. *Histopathology* **38**, 120–134 (2001).
13. G. K. Gouras *et al.*, Intraneuronal Abeta42 accumulation in human brain. *Am. J. Pathol.* **156**, 15–20 (2000).
14. F. M. LaFerla, J. C. Troncoso, D. K. Strickland, C. H. Kawas, G. Jay, Neuronal cell death in Alzheimer's disease correlates with apoE uptake and intracellular Abeta stabilization. *J. Clin. Invest.* **100**, 310–320 (1997).
15. L. A. Welikovitch *et al.*, Evidence of intraneuronal Aβ accumulation preceding tau pathology in the entorhinal cortex. *Acta Neuropathol.* **136**, 901–917 (2018).
16. F. Bao *et al.*, Different β-amyloid oligomer assemblies in Alzheimer brains correlate with age of disease onset and impaired cholinergic activity. *Neurobiol. Aging* **33**, 825.e1–813 (2012).
17. E. N. Cline, M. A. Bicca, K. L. Viola, W. L. Klein, The Amyloid-β oligomer hypothesis: Beginning of the third decade. *J. Alzheimers Dis.* **64** (supp. 1), S567–S610 (2018).
18. D. J. Koss *et al.*, Soluble pre-fibrillar tau and β-amyloid species emerge in early human Alzheimer's disease and track disease progression and cognitive decline. *Acta Neuropathol.* **132**, 875–895 (2016).
19. L. F. Lue *et al.*, Soluble amyloid beta peptide concentration as a predictor of synaptic change in Alzheimer's disease. *Am. J. Pathol.* **155**, 853–862 (1999).
20. C. A. McLean *et al.*, Soluble pool of Abeta amyloid as a determinant of severity of neurodegeneration in Alzheimer's disease. *Ann. Neurol.* **46**, 860–866 (1999).
21. R. H. Takahashi *et al.*, Intraneuronal Alzheimer abeta42 accumulates in multivesicular bodies and is associated with synaptic pathology. *Am. J. Pathol.* **161**, 1869–1879 (2002).
22. R. M. Cohen *et al.*, A transgenic Alzheimer rat with plaques, tau pathology, behavioral impairment, oligomeric aβ, and frank neuronal loss. *J. Neurosci.* **33**, 6245–6256 (2013).
23. S. Oddo *et al.*, Triple-transgenic model of Alzheimer's disease with plaques and tangles: Intracellular Abeta and synaptic dysfunction. *Neuron* **39**, 409–421 (2003).
24. Y. Qi *et al.*, Longitudinal testing of hippocampal plasticity reveals the onset and maintenance of endogenous human Aβ-induced synaptic dysfunction in individual freely behaving pre-plaque transgenic rats: Rapid reversal by anti-Aβ agents. *Acta Neuropathol. Commun.* **2**, 175 (2014).
25. L. M. Billings, S. Oddo, K. N. Green, J. L. McGaugh, F. M. LaFerla, Intraneuronal Abeta causes the onset of early Alzheimer's disease-related cognitive deficits in transgenic mice. *Neuron* **45**, 675–688 (2005).
26. V. Echeverria *et al.*, Altered mitogen-activated protein kinase signaling, tau hyperphosphorylation and mild spatial learning dysfunction in transgenic rats expressing the beta-amyloid peptide intracellularly in hippocampal and cortical neurons. *Neuroscience* **129**, 583–592 (2004).
27. M. T. Ferretti *et al.*, Transgenic mice as a model of pre-clinical Alzheimer's disease. *Curr. Alzheimer Res.* **8**, 4–23 (2011).
28. P. Galeano *et al.*, Longitudinal analysis of the behavioral phenotype in a novel transgenic rat model of early stages of Alzheimer's disease. *Front. Behav. Neurosci.* **8**, 321 (2014).
29. M. F. Iulita *et al.*, Intracellular Aβ pathology and early cognitive impairments in a transgenic rat overexpressing human amyloid precursor protein: A multidimensional study. *Acta Neuropathol. Commun.* **2**, 61 (2014).

30. W. C. Leon *et al*., A novel transgenic rat model with a full Alzheimer's-like amyloid pathology displays pre-plaque intracellular amyloid-beta-associated cognitive impairment. *J. Alzheimers Dis.* **20**, 113–126 (2010).
31. T. Petrasek *et al*., The McGill transgenic rat model of Alzheimer's disease displays cognitive and motor impairments, changes in anxiety and social behavior, and altered circadian activity. *Front. Aging Neurosci.* **10**, 250 (2018).
32. M. T. Ferretti, S. Allard, V. Partridge, A. Ducatenzeiler, A. C. Cuello, Minocycline corrects early, pre-plaque neuroinflammation and inhibits BACE-1 in a transgenic model of Alzheimer's disease-like amyloid pathology. *J. Neuroinflammation* **9**, 62 (2012).
33. C. E. Hanzel *et al*., Neuronal driven pre-plaque inflammation in a transgenic rat model of Alzheimer's disease. *Neurobiol. Aging* **35**, 2249–2262 (2014).
34. I. Heggland, I. S. Storkaas, H. T. Soligard, A. Kobro-Flatmoen, M. P. Witter, Stereological estimation of neuron number and plaque load in the hippocampal region of a transgenic rat model of Alzheimer's disease. *Eur. J. Neurosci.* **41**, 1245–1262 (2015).
35. M. T. Heneka *et al*., Focal glial activation coincides with increased BACE1 activation and precedes amyloid plaque deposition in APP[V717I] transgenic mice. *J. Neuroinflammation* **2**, 22 (2005).
36. M. C. Janelsins *et al*., Early correlation of microglial activation with enhanced tumor necrosis factor-alpha and monocyte chemoattractant protein-1 expression specifically within the entorhinal cortex of triple transgenic Alzheimer's disease mice. *J. Neuroinflammation* **2**, 23 (2005).
37. M. T. Ferretti, M. A. Bruno, A. Ducatenzeiler, W. L. Klein, A. C. Cuello, Intracellular Aβ-oligomers and early inflammation in a model of Alzheimer's disease. *Neurobiol. Aging* **33**, 1329–1342 (2012).
38. E. N. Wilson *et al*., Microdose lithium NP03 diminishes pre-plaque oxidative damage and neuroinflammation in a rat model of Alzheimer's-like amyloidosis. *Curr. Alzheimer Res.* **15**, 1220–1230 (2018).
39. M. A. Lynch, The multifaceted profile of activated microglia. *Mol. Neurobiol.* **40**, 139–156 (2009).
40. C. Mori *et al*., Intraneuronal Abeta42 accumulation in Down syndrome brain. *Amyloid* **9**, 88–102 (2002).
41. S. M. Grant, A. Ducatenzeiler, M. Szyf, A. C. Cuello, Abeta immunoreactive material is present in several intracellular compartments in transfected, neuronally differentiated, P19 cells expressing the human amyloid beta-protein precursor. *J. Alzheimers Dis.* **2**, 207–222 (2000).
42. L. Bertram, R. E. Tanzi, Alzheimer disease risk genes: 29 and counting. *Nat. Rev. Neurol.* **15**, 191–192 (2019).
43. C. M. Karch, A. M. Goate, Alzheimer's disease risk genes and mechanisms of disease pathogenesis. *Biol. Psychiatry* **77**, 43–51 (2015).
44. S. A. Liddelow *et al*., Neurotoxic reactive astrocytes are induced by activated microglia. *Nature* **541**, 481–487 (2017).
45. L. Peferoen, M. Kipp, P. van der Valk, J. M. van Noort, S. Amor, Oligodendrocyte-microglia cross-talk in the central nervous system. *Immunology* **141**, 302–313 (2014).
46. J. Brelstaff, A. M. Tolkovsky, B. Ghetti, M. Goedert, M. G. Spillantini, Living neurons with tau filaments aberrantly expose phosphatidylserine and are phagocytosed by microglia. *Cell Rep.* **24**, 1939–1948.e4 (2018).
47. E. S. Drummond, S. Nayak, B. Ueberheide, T. Wisniewski, Proteomic analysis of neurons microdissected from formalin-fixed, paraffin-embedded Alzheimer's disease brain tissue. *Sci. Rep.* **5**, 15456 (2015).
48. S. D. Ginsberg, M. J. Alldred, S. Che, Gene expression levels assessed by CA1 pyramidal neuron and regional hippocampal dissections in Alzheimer's disease. *Neurobiol. Dis.* **45**, 99–107 (2012).
49. S. D. Ginsberg *et al*., Microarray analysis of hippocampal CA1 neurons implicates early endosomal dysfunction during Alzheimer's disease progression. *Biol. Psychiatry* **68**, 885–893 (2010).
50. D. C. Hondius *et al*., Profiling the human hippocampal proteome at all pathologic stages of Alzheimer's disease. *Alzheimers Dement.* **12**, 654–668 (2016).
51. W. S. Liang *et al*., Neuronal gene expression in non-demented individuals with intermediate Alzheimer's disease neuropathology. *Neurobiol. Aging* **31**, 549–566 (2010).
52. S. Du Yan *et al*., Amyloid-beta peptide-receptor for advanced glycation endproduct interaction elicits neuronal expression of macrophage-colony stimulating factor: A proinflammatory pathway in Alzheimer disease. *Proc. Natl. Acad. Sci. U.S.A.* **94**, 5296–5301 (1997).
53. G. M. Murphy, Jr, F. Zhao, L. Yang, B. Cordell, Expression of macrophage colony-stimulating factor receptor is increased in the AbetaPP(V717F) transgenic mouse model of Alzheimer's disease. *Am. J. Pathol.* **157**, 895–904 (2000).
54. A. Sokolova *et al*., Monocyte chemoattractant protein-1 plays a dominant role in the chronic inflammation observed in Alzheimer's disease. *Brain Pathol.* **19**, 392–398 (2009).
55. M. Q. Xia, S. X. Qin, L. J. Wu, C. R. Mackay, B. T. Hyman, Immunohistochemical study of the beta-chemokine receptors CCR3 and CCR5 and their ligands in normal and Alzheimer's disease brains. *Am. J. Pathol.* **153**, 31–37 (1998).
56. L. Ho *et al*., Elevated plasma MCP-1 concentration following traumatic brain injury as a potential "predisposition" factor associated with an increased risk for subsequent development of Alzheimer's disease. *J. Alzheimers Dis.* **31**, 301–313 (2012).
57. K. Ishizuka *et al*., Identification of monocyte chemoattractant protein-1 in senile plaques and reactive microglia of Alzheimer's disease. *Psychiatry Clin. Neurosci.* **51**, 135–138 (1997).
58. A. Olmos-Alonso *et al*., Pharmacological targeting of CSF1R inhibits microglial proliferation and prevents the progression of Alzheimer's-like pathology. *Brain* **139**, 891–907 (2016).
59. M. Haskins, T. E. Jones, Q. Lu, S. K. Bareiss, Early alterations in blood and brain RANTES and MCP-1 expression and the effect of exercise frequency in the 3xTg-AD mouse model of Alzheimer's disease. *Neurosci. Lett.* **610**, 165–170 (2016).
60. D. Galimberti *et al*., Serum MCP-1 levels are increased in mild cognitive impairment and mild Alzheimer's disease. *Neurobiol. Aging* **27**, 1763–1768 (2006).
61. D. Galimberti *et al*., Intrathecal chemokine synthesis in mild cognitive impairment and Alzheimer disease. *Arch. Neurol.* **63**, 538–543 (2006).
62. A. R. Morgan *et al*.; NIMA Consortium; Annex: NIMA–Wellcome Trust Consortium for Neuroimmunology of Mood Disorders and Alzheimer's Disease, Inflammatory biomarkers in Alzheimer's disease plasma. *Alzheimers Dement.* **15**, 776–787 (2019).
63. R. Zhang *et al*., Systemic immune system alterations in early stages of Alzheimer's disease. *J. Neuroimmunol.* **256**, 38–42 (2013).
64. W. J. Lee *et al*., Plasma MCP-1 and cognitive decline in patients with Alzheimer's disease and mild cognitive impairment: A two-year follow-up study. *Sci. Rep.* **8**, 1280 (2018).
65. K. Westin *et al*., CCL2 is associated with a faster rate of cognitive decline during early stages of Alzheimer's disease. *PLoS One* **7**, e30525 (2012).
66. B. M. Bettcher *et al*., MCP-1 and eotaxin-1 selectively and negatively associate with memory in MCI and Alzheimer's disease dementia phenotypes. *Alzheimers Dement. (Amst.)* **3**, 91–97 (2016).
67. B. M. Bettcher *et al*., Increases in a pro-inflammatory chemokine, MCP-1, are related to decreases in memory over time. *Front. Aging Neurosci.* **11**, 25 (2019).
68. J. A. Pillai *et al*.; Alzheimer's Disease Neuroimaging Initiative, Key inflammatory pathway activations in the MCI stage of Alzheimer's disease. *Ann. Clin. Transl. Neurol.* **6**, 1248–1262 (2019).
69. S. C. Burnham *et al*.; Alzheimer's Disease Neuroimaging Initiative; Australian Imaging, Biomarkers and Lifestyle Study Research Group, A blood-based predictor for neocortical Aβ burden in Alzheimer's disease: Results from the AIBL study. *Mol. Psychiatry* **19**, 519–526 (2014).
70. V. A. Vincent, S. P. Selwood, G. M. Murphy, Jr, Proinflammatory effects of M-CSF and A beta in hippocampal organotypic cultures. *Neurobiol. Aging* **23**, 349–362 (2002).
71. M. Rentzos *et al*., Interleukin-12 is reduced in cerebrospinal fluid of patients with Alzheimer's disease and frontotemporal dementia. *J. Neurol. Sci.* **249**, 110–114 (2006).
72. E. Rota *et al*., Increased intrathecal TGF-beta1, but not IL-12, IFN-gamma and IL-10 levels in Alzheimer's disease patients. *Neurol. Sci.* **27**, 33–39 (2006).
73. A. Boza-Serrano, Y. Yang, A. Paulus, T. Deierborg, Innate immune alterations are elicited in microglial cells before plaque deposition in the Alzheimer's disease mouse model 5xFAD. *Sci. Rep.* **8**, 1550 (2018).
74. D. Davalos *et al*., ATP mediates rapid microglial response to local brain injury in vivo. *Nat. Neurosci.* **8**, 752–758 (2005).
75. A. Nimmerjahn, F. Kirchhoff, F. Helmchen, Resting microglial cells are highly dynamic surveillants of brain parenchyma in vivo. *Science* **308**, 1314–1318 (2005).
76. H. Kettenmann, U. K. Hanisch, M. Noda, A. Verkhratsky, Physiology of microglia. *Physiol. Rev.* **91**, 461–553 (2011).
77. H. Wake, A. J. Moorhouse, S. Jinno, S. Kohsaka, J. Nabekura, Resting microglia directly monitor the functional state of synapses in vivo and determine the fate of ischemic terminals. *J. Neurosci.* **29**, 3974–3980 (2009).
78. M. Kuijpers, K. L. van Gassen, P. N. de Graan, D. Gruol, Chronic exposure to the chemokine CCL3 enhances neuronal network activity in rat hippocampal cultures. *J. Neuroimmunol.* **229**, 73–80 (2010).
79. E. Marciniak *et al*., The Chemokine MIP-1α/CCL3 impairs mouse hippocampal synaptic transmission, plasticity and memory. *Sci. Rep.* **5**, 15862 (2015).
80. E. N. Wilson *et al*., Intraneuronal amyloid beta accumulation disrupts hippocampal CRTC1-dependent gene expression and cognitive function in a rat model of Alzheimer disease. *Cereb. Cortex* **27**, 1501–1511 (2017).
81. E. N. Wilson *et al*., BACE1 inhibition by microdose lithium formulation NP03 rescues memory loss and early stage amyloid neuropathology. *Transl. Psychiatry* **7**, e1190 (2017).
82. I. L. Gutiérrez *et al*., Reboxetine treatment reduces neuroinflammation and neurodegeneration in the 5xFAD mouse model of Alzheimer's disease: Role of CCL2. *Mol. Neurobiol.* **56**, 8628–8642 (2019).
83. T. Kiyota *et al*., AAV1/2-mediated CNS gene delivery of dominant-negative CCL2 mutant suppresses gliosis, beta-amyloidosis, and learning impairment of APP/PS1 mice. *Mol. Ther.* **17**, 803–809 (2009).
84. G. Di Liberto *et al*., Neurons under T cell attack coordinate phagocyte-mediated synaptic stripping. *Cell* **175**, 458–471.e19 (2018).
85. C. Cserep *et al*., Microglia monitor and protect neuronal function through specialized somatic purinergic junctions. *Science* **367**, 528–537 (2020).
86. P. V. Arriagada, J. H. Growdon, E. T. Hedley-Whyte, B. T. Hyman, Neurofibrillary tangles but not senile plaques parallel duration and severity of Alzheimer's disease. *Neurology* **42**, 631–639 (1992).
87. A. D. Dayan, Quantitative histological studies on the aged human brain. II. Senile plaques and neurofibrillary tangles in senile dementia (with an appendix on their occurrence in cases of carcinoma). *Acta Neuropathol.* **16**, 95–102 (1970).
88. S. T. DeKosky, S. W. Scheff, Synapse loss in frontal cortex biopsies in Alzheimer's disease: Correlation with cognitive severity. *Ann. Neurol.* **27**, 457–464 (1990).
89. W. Samuel, R. D. Terry, R. DeTeresa, N. Butters, E. Masliah, Clinical correlates of cortical and nucleus basalis pathology in Alzheimer dementia. *Arch. Neurol.* **51**, 772–778 (1994).
90. R. D. Terry *et al*., Physical basis of cognitive alterations in Alzheimer's disease: Synapse loss is the major correlate of cognitive impairment. *Ann. Neurol.* **30**, 572–580 (1991).
91. G. K. Wilcock, M. M. Esiri, Plaques, tangles and dementia. A quantitative study. *J. Neurol. Sci.* **56**, 343–356 (1982).